The Two-pore channel (TPC) interactome unmasks isoform-specific roles for TPCs in endolysosomal morphology and cell pigmentation

Yaping Lin-Moshier[a], Michael V. Keebler[a], Robert Hooper[b], Michael J. Boulware[a], Xiaolong Liu[a], Dev Churamani[b], Mary E. Abood[c], Timothy F. Walseth[a], Eugen Brailoiu[c], Sandip Patel[b], and Jonathan S. Marchant[a,1]

[a]Department of Pharmacology, University of Minnesota, Minneapolis, MN 55455; [b]Department of Cell and Developmental Biology, University College London, London WC1E 6BT, United Kingdom; and [c]Departments of Anatomy, Cell Biology, and Pharmacology and the Center for Substance Abuse, Temple University School of Medicine, Philadelphia, PA 19140

Edited by Richard W. Aldrich, University of Texas at Austin, Austin, TX, and approved July 30, 2014 (received for review April 20, 2014)

The two-pore channels (TPC1 and TPC2) belong to an ancient family of intracellular ion channels expressed in the endolysosomal system. Little is known about how regulatory inputs converge to modulate TPC activity, and proposed activation mechanisms are controversial. Here, we compiled a proteomic characterization of the human TPC interactome, which revealed that TPCs complex with many proteins involved in Ca^{2+} homeostasis, trafficking, and membrane organization. Among these interactors, TPCs were resolved to scaffold Rab GTPases and regulate endomembrane dynamics in an isoform-specific manner. TPC2, but not TPC1, caused a proliferation of endolysosomal structures, dysregulating intracellular trafficking, and cellular pigmentation. These outcomes required both TPC2 and Rab activity, as well as their interactivity, because TPC2 mutants that were inactive, or rerouted away from their endogenous expression locale, or deficient in Rab binding, failed to replicate these outcomes. Nicotinic acid adenine dinucleotide phosphate (NAADP)-evoked Ca^{2+} release was also impaired using either a Rab binding-defective TPC2 mutant or a Rab inhibitor. These data suggest a fundamental role for the ancient TPC complex in trafficking that holds relevance for lysosomal proliferative scenarios observed in disease.

Ca^{2+} signaling | lysosome | Xenopus

Two-pore channels (TPCs) are an ancient family of intracellular ion channels and a likely ancestral stepping stone in the evolution of voltage-gated Ca^{2+} and Na^{+} channels (1). Architecturally, TPCs resemble a halved voltage-gated Ca^{2+}/Na^{+} channel with cytosolic NH_2 and COOH termini, comprising two repeats of six transmembrane spanning helices with a putative pore-forming domain between the fifth and sixth membrane-spanning regions. Since their discovery in vertebrate systems, many studies have investigated the properties of these channels (2–7) that may support such a lengthy evolutionary pedigree.

In this context, demonstration that (*i*) the two human TPC isoforms (TPC1 and TPC2) are uniquely distributed within the endolysosomal system (2, 3) and that (*ii*) TPC channel activity is activated by the Ca^{2+} mobilizing molecule nicotinic acid adenine dinucleotide phosphate (NAADP) (4–6) generated considerable excitement that TPCs function as effectors of this mercurial second messenger long known to trigger Ca^{2+} release from "acidic stores." The spectrum of physiological activities that have been linked to NAADP signaling over the last 25 years (8, 9) may therefore be realized through regulation of TPC activity. However, recent studies have questioned the idea that TPCs are NAADP targets (10, 11), demonstrating instead that TPCs act as Na^{+} channels regulated by the endolysosomal phosphoinositide $PI(3,5)P_2$. Such controversy (12, 13) underscores how little we know about TPC regulatory inputs and the dynamic composition of TPC complexes within cells.

Here, to generate unbiased insight into the cell biology of the TPC complex, we report a proteomic analysis of human TPCs. The TPC interactome establishes a useful community resource as a "rosetta stone" for interrogating the cell biology of TPCs and their regulation. The dataset reveals a predomination of links between TPCs and effectors controlling membrane organization and trafficking, relevant for disease states involving lysosomal proliferation where TPC functionality may be altered (14).

Results

TPC Affinity Purification. For affinity purification, we used a method based upon "One-*Strep*"-tagging (Fig. 1*A*). This method uses a short (~2 kDa), stable tag exhibiting high affinity for an engineered streptavidin (*Strep*-Tactin) to enable one-step purification of TPC complexes. The utility of this approach for defining protein interactomes (including dynamic, transient interactions) has been shown in several applications (15) and is outlined schematically in Fig. 1*B*. Potential TPC-interacting candidates, with matched sections from control lanes, were processed for identification by mass spectrometry (Fig. 1*C*). Common hits, absent from controls, were then used to define the basal TPC interactome. Table 1 collates common TPC interactors prioritized by total peptide number (greater than five peptides in experimental samples and absence from controls). Unique TPC1/2 interactors (greater than five peptides in experimental samples and absence from the alternate isoform purification) are shown in Table S1.

The quality of the proteomic dataset was interrogated in several ways. First, the predominance and coverage of bait (TPCs) in dataset (and absence from controls) was assessed. TPCs were the predominant protein found in their respective purification datasets (peptide coverage was >60% of the predicted non-transmembrane regions for both TPCs) (Fig. S1). Second,

Significance

Two-pore channels (TPCs) are a recently discovered family of endolysosomal ion channels, but their regulation is controversial. By defining the TPC interactome, we provide a community resource that illuminates TPC complex regulation and resolves associations with novel partners and processes. Physical interactions with endolysosomal trafficking regulators predominate, and Rab GTPases impart isoform-specific roles for TPCs in organelle proliferation and cellular pigmentation. These data imply a fundamental role for TPCs in trafficking that augurs significance for disease states exhibiting lysosomal proliferation where TPC dysregulation may drive pathogenesis.

Author contributions: Y.L.-M., S.P., and J.S.M. designed research; Y.L.-M., M.V.K., R.H., M.J.B., X.L., D.C., M.E.A., T.F.W., E.B., S.P., and J.S.M. performed research; Y.L.-M., M.V.K., R.H., M.J.B., X.L., D.C., M.E.A., T.F.W., E.B., S.P., and J.S.M. analyzed data; and Y.L.-M. and J.S.M. wrote the paper.

The authors declare no conflict of interest.

This article is a PNAS Direct Submission.

Freely available online through the PNAS open access option.

[1]To whom correspondence should be addressed. Email: march029@umn.edu.

This article contains supporting information online at www.pnas.org/lookup/suppl/doi:10.1073/pnas.1407004111/-/DCSupplemental.

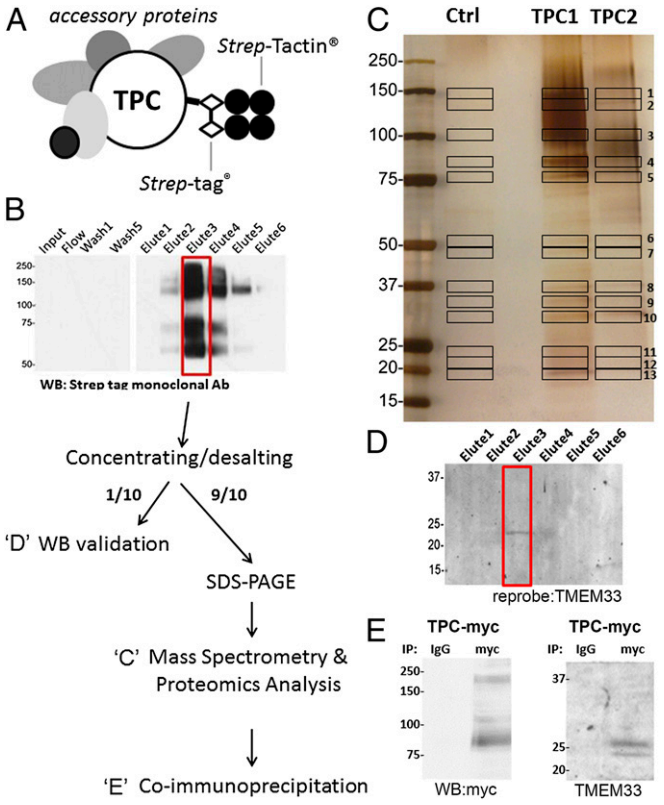

Fig. 1. Strategy for affinity purification and validation of TPC interactors. (*A*) Diagram of affinity purification method that illustrates TPC (open) and TPC-associated protein complexes (shaded) binding to *Strep*-Tactin via the *Strep*-tag moiety. (*B*) TPC isolation followed the same protocol for TPC1/2 purifications with elution of TPC complexes tracked via an anti–*Strep*-tag monoclonal. (*Upper*) Representative purification followed by Western blot detection (anti–*Strep*-tag) of TPC2 protein in specific eluates. (*Lower*) Schematic showing eluate "3" was processed for SDS/PAGE and mass spectrometry ("C"). Validation of interactors was performed by Western blotting of TPC-enriched eluates ("D") and coimmunoprecipitation ("E"). (*C*) Example of silver-stained gel highlighting positions of excised bands in TPC1/2 purifications together with bands cut from equivalent positions in controls (no *Strep*-tag). (*D*) Western blot for endogenous TMEM33, a representative interactor. (*E*) Interaction between endogenous TMEM33 and TPC confirmed by coimmunoprecipitation in HEK293 cells expressing TPC1-MYC.

candidate TPC interactors assigned by mass spectrometry were validated by (*i*) screening for presence in the TPC-enriched eluate (Fig. 1*D*) before (*ii*) interactivity was assessed by coimmunoprecipitation (Fig. 1*E*). These steps are exemplified for TMEM33, one candidate TPC interactor. Third, the entire purification dataset was cross-referenced with in silico datasets to ascertain potential interactivity. This analysis revealed a dense web of putative interactions (Fig. 2*A*). Fourth, the unbiased purification dataset was interrogated for recently evidenced TPC interactors: both HAX1 (16) and mTOR (11) were present in the dataset (Table 1). Finally, approximately half the identified proteins exhibited well-validated endolysosomal localizations. Collectively, these outcomes support the specificity of this approach.

Definition of the TPC Interactome. Pathway analysis of the TPC interactome revealed several functional groupings. First were candidates linking TPCs to Ca^{2+} homeostasis. Relevant interactors encompass Ca^{2+} binding proteins (annexins, calreticulin, reticulocalbin, CHP), TMEM165 (an organellar Ca^{2+}/H^{+} antiporter) (17), SURF4 (a STIM1 interactor) (18), and IP_3R interactors (ATP1A1 and MYH9) (19, 20).

Second is a grouping of proteins involved in membrane trafficking and organization (Rab GTPases, syntaxins, synaptogyrins, annexins, and sigma receptors). Rab GTPases, small monomeric GTPases that control intracellular trafficking (21, 22), predominated in terms of peptide number (Table 1) and interactivity

Table 1. Common TPC interactors

No.	Candidate description	Gene name	Peptide no. Control	Peptide no. TPC1 and -2
	TPC2	**TPCN2**	**5**	**282**
	TPC1	**TPCN1**	**1**	**254**
1	Na/K-transporting ATPase subunit alpha-1	ATP1A1	0	132
2	**Rab GTPase family**	**RAB**	**0**	**129**
3	Transmembrane emp24 domain family	TMED1-5, 7, 9, 10	0	98
4	3-Hydroxyacyl-CoA dehydratase 3	PTPLAD1	0	65
5	Surfeit locus protein 4	SURF4	0	55
6	ADP/ATP translocase	SLC25A5/6	0	54
7	**Membrane-associated progesterone receptor component 1**	**PGRMC1**	**0**	**49**
8	Isoform 2, 4F2 cell-surface antigen heavy chain	SLC3A2	0	42
9	Aldolase A	ALDOA	0	40
10	**Annexin family**	ANXA1-7,11	**0**	**40**
11	Transmembrane 9 superfamily	TM9SF1-3	0	38
12	Peroxiredoxin Family	PRDX1,4,6	0	38
13	Transmembrane protein 33	TMEM33	0	36
14	**Rab GDP dissociation inhibitor beta**	**GDI2**	**0**	**33**
15	VDAC family	VDAC1-3	0	31
16	Myosin, heavy chain 9	MYH9	0	30
17	Prohibitin-2	PHB2	0	30
18	Transmembrane protein 165	TM165	0	26
19	Isoform 2, magnesium transporter MRS2 homolog	MRS2	0	23
20	Ceramide synthase 2	CERS2	0	22
21	Sideroflexin family	SFXN1,2,4	0	21
22	Ancient ubiquitous protein	AUP1	0	21
23	Large neutral amino acids transporter small subunit 1	SLC7A5	0	20
24	Ca-binding protein p22	CHP	0	18
25	Vesicular integral protein36	VIP36	0	17
26	Isoform ADelta10 of prelamin-A/C	LMNA	0	16
27	Reticulocalbin-2	RCN2	0	16
28	Inorganic pyrophosphatase	PPA1	0	15
29	Isoform 2, heat shock protein 90α	HSP90AA1	0	14
30	Isoform 2, adenylyl cyclase-associated protein 1	CAP1	0	14
31	**Synaptogyrin family**	SYNGR 2,3	**0**	**12**
32	Calreticulin	CALR	0	10
33	Isoform 3, probable hydrolase	PNKD	0	10
34	**Syntaxin Family**	STX16,18	**0**	**9**
35	BAG family molecular chaperone regulator 2	BAG2	0	9
36	Fat storage-inducing transmembrane protein 2	FITM2	0	8
37	Serine/threonine-protein kinase mTOR	MTOR	0	8
38	Ataxin-2-like protein	ATXN2L	0	8
39	**Isoform 3, sigma receptor 1**	SGMR1	**0**	**6**
40	Isoform 2, HCLS1-associated protein X-1	HAX1	0	6

Bolded entries highlight candidates involved in trafficking and/or membrane organization.

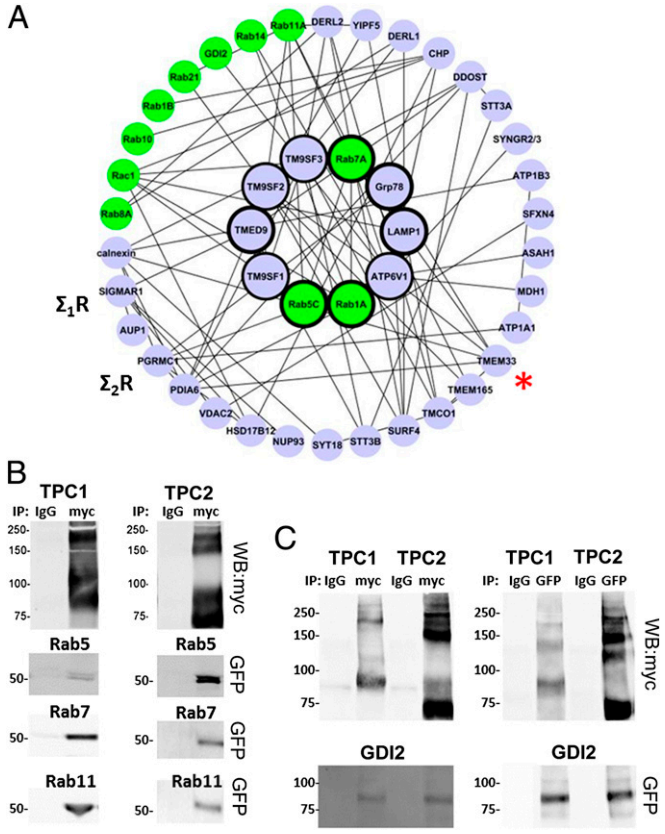

Fig. 2. Interactivity analysis and validation of TPC interactors. (*A*) TPC interactome. Spoke density reveals linkage between subsets of nodes based on predicted in silico interactions by FunCoup. Center wheel comprises proteins with biologically well-verified endolysosomal localizations. Other proteins fulfilling criteria as interactors, but currently lacking in vivo evidence of localization with acidic stores, are shown in the outer wheel. Rab GTPases (green circles) were a large interactor clade. Other highlighted interactors discussed in *Results* include sigma receptors (Σ_1R, Σ_2R) and TMEM33 (*) (Fig. 1). (*B*) Coimmunoprecipitation of TPC1 (*Left*) and TPC2 (*Right*) with Rab GTPases. Rab constructs were tagged with GFP and expressed in HEK293 cells together with MYC-tagged TPCs. (*C*) Coimmunoprecipitation of TPCs and GDI2. (*Left*) GFP-tagged GDI2 was detected in MYC-TPC complexes in HEK293 whole-cell lysates. (*Right*) Reciprocal coimmunoprecipitation.

analysis (Fig. 2*A*, green circles). Several Rab family members regulate endolysosomal dynamics (including Rab5, Rab7, and Rab11) (21–24), and a broad spectrum of Rabs (>100 peptide hits), as well as a Rab GDP dissociation inhibitor (GDI2), were resolved as candidate interactors (Table 1). Rabs are known to associate with ion channels (25), including voltage-gated Ca^{2+} channels with which TPCs share homology (26). Other interactors impacting membrane organization included the sigma receptors (Σ_1R and Σ_2R). Σ_1R is an intracellular receptor and chaperone that associates with ion channels including voltage-gated Ca^{2+} channels (27) and IP_3Rs at organellar contact sites (28). Less is known about Σ_2R [progesterone receptor membrane component 1 (PGRMC1)] (29), but results with fluorescently labeled Σ_2R ligands show a presence in lysosomes (30) consistent with effects of Σ_2R ligands on lysosomal permeability and Ca^{2+} release from thapsigargin-insensitive Ca^{2+} stores (31, 32).

Third, several interactors are autophagy regulators. These candidates include the poorly characterized endolysosomal nonaspanins (TM9SF1-3) (33) (which regulate autophagosome formation), MYH9 (34), annexins (35), and the SLC7A5-SLC3A2 antiporter, which activates mTORC1, a known TPC interactor (11).

Functional Interaction with Rab GTPases. As a first step toward validating the functional significance of interactors from within this large dataset, we focused on Rab GTPases (Fig. 2). Rab7 regulates neuronal vesicle trafficking and neurite outgrowth (36), just like NAADP (37). Rab proteins also regulate autophagy (38), just like NAADP (39). Alterations in Rab activity yield pigmentation defects (40) as do TPC2 sequence variants (41). A regulatory convergence of Rabs and NAADP on TPCs may therefore provide a common molecular basis for these effects.

Coimmunoprecipitation confirmed an interaction between both TPCs and several Rab isoforms (Fig. 2*B* and Fig. S2) consistent with the broad specificity of known Rab-binding motifs (42). TPCs were able to interact with Rabs in multiple stages of the Rab cycle (Fig. S3). Colocalization, as exemplified for Rab7A, was supported by live cell confocal imaging (Fig. S4). Interactivity between TPCs and GDI2, another proteomic candidate (Table 1), was also validated (Fig. 2*C*).

To investigate the functional impact of this association, we expressed TPCs in *Xenopus* oocytes as a simple model for studying trafficking events (43). Surprisingly, TPC2 expression disrupted pigment distribution at the apex of the heavily pigmented animal hemisphere, giving the oocyte a "balding" appearance. This effect was particularly clear in cells expressing TPC2-GFP, as intracellular TPC2-GFP fluorescence became obvious as the attenuatory effect of melanosomes was disrupted (Fig. 3*A*). Incubation of TPC2-injected cells with a Rab7 nucleotide binding inhibitor (44) caused a concentration-dependent inhibition of the pigment phenotype (Fig. 3*H*), suggesting that a functional interaction with Rab GTPases supports this phenomenon. Reciprocally, the pigmentation phenotype also required TPC2 activity. No pigment defect was observed in oocytes expressing a TPC2-pore mutant (TPC2 [L265P]) (5) that ablated channel activity (Fig. 3*A*), or following incubation in BAPTA-AM (Fig. S5). Therefore, this simple *Xenopus* assay revealed a TPC2-evoked pigmentation defect dependent upon both Rab7 and TPC2 activity, as well as local Ca^{2+} changes.

Confocal imaging analyses also revealed an underlying intracellular trafficking defect in TPC2-expressing cells. TPC2 cells uniquely displayed a proliferation of vesicular structures in the oocyte subcortex beneath the cortical ER (arrows in Fig. 3*B*), that was not observed in oocytes expressing the pore mutant TPC2[L265P]. These structures were easily resolved in lateral (*xy*) or axial (*xz*) section (Fig. 3*B*) and higher magnification images revealed them as vesicular aggregates resembling "bunches of grapes" (Fig. 3*C*). Quantification of this TPC2-evoked effect was made by measuring the size of these structures in cells expressing TPC2 versus TPC2[L265P]. This comparison was performed via a simple ratio of the average population means of vesicular size between two confocal planes taken within, and beneath, the cortical ER (Fig. 3*D*). Only in TPC2-positive cells were these larger aggregates observed, skewing this ratio of population means to higher values compared with TPC2 [L265P] expressing cells (Fig. 3*E*). Therefore, overexpression of TPC2 elicited a vesicular aggregation phenotype, seen only in cells with the pigment defect, and again this outcome required TPC2 functionality.

Although these effects require Rab and TPC activity, do they require Rab and TPC interactivity? Given the cytoplasmic localization of both the NH_2 (N_{ter}) and COOH (C_{ter}) regions of TPC (45) and prior precedent for the interaction of Rabs within the termini of ion channels (25), we investigated the role of these regions in binding Rab7A, an endolysosomal Rab shown to interact with both TPCs (Fig. 2*B*). Coimmunoprecipitation assays were performed using GFP-Rab7A together with MYC-tagged NH_2- or COOH-terminal domains of TPC2 (N_{ter}-TPC2 and C_{ter}-TPC2) (Fig. 3*F*). No association was detected between C_{ter}-TPC2 and GFP-Rab7 whereas GFP-Rab7 was recovered with N_{ter}-TPC2 (Fig. 3*F*). Moreover, point mutations within the TPC2 NH_2-terminal domain of a motif ("QVGPG" to "aaGaG", residues 33–37, N_{ter}[RBDaaa]) conforming to the consensus of a GTPase binding and trafficking module (Q/R/KVxPx)

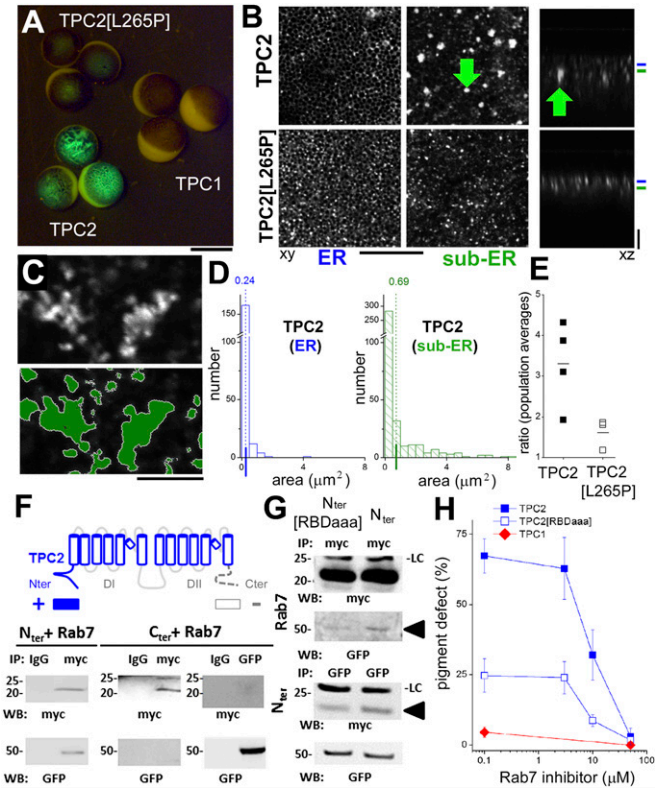

Fig. 3. Pigment perturbation and organelle proliferation in TPC2-expressing cells. (*A*) Epifluorescence images of *Xenopus* oocytes taken 48 h after expression of GFP-tagged constructs. (Scale bar: 1 mm.) (*B*) Lateral ("*xy*," *Left* and *Center*) and axial ("*xz*," *Right*) images of TPC2 (*Upper*) and TPC2 pore mutant (TPC2[L265P], *Lower*) expression at the level of (blue) and beneath (green) cortical ER. Arrow, vesicular aggregates in TPC2-expressing cells in the subcortical ER. (Scale bars: "xy," 30 μm; "xz," 15 μm.) (*C*) Higher resolution image of aggregates in TPC2 cells (*Upper*) and morphometric analysis (*Lower*). The green area was quantified for analyses shown in *D*. (Scale bar: 2.5 μm.) (*D*) Histograms of vesicular size at the ER (blue) and sub-ER level (green) highlighting large vesicular aggregates in TPC2-expressing cells. (*E*) Morphometric comparison of TPC2 and TPC2[L265P] expressing structures via a ratio of population means of organelle size at two focal planes for TPC2 (for example, 0.69/0.24 from *D*) and TPC2[L265P]. (*F*) Rab7 interaction site(s) within TPC2. Schematic of TPC topology shows the two domain organization (DI, DII) with cytoplasmic NH_2 (N_{ter}) and COOH (C_{ter}) termini. Regions screened positive (+, color) and negative (–, gray) for Rab7 interactivity from coimmunoprecipitation assays are highlighted as boxes. (*Lower*) Coimmunoprecipitation blots for MYC (*Upper*) and GFP (*Lower*) epitopes. The N_{ter} of TPC2 binds Rab7, but reciprocal co-IPs at the COOH terminus failed to detect an interaction. (*G*) Coimmunoprecipitation with two NH_2-terminal TPC2 domain fragments (N_{ter}[RBDaaa] and N_{ter}). Rab7 interaction was impaired in the N_{ter}[RBDaaa] mutant (arrowheads) when assessed by reciprocal coimmunoprecipitation. LC, light chain. (*H*) Pigment phenotype in TPC-expressing oocytes in the presence of indicated concentrations of Rab7 inhibitor (Rab-I, CID1067700). Data represent means ± SEM.

(46) reduced Rab7 association with the NH_2 terminus of TPC2 (>70%) (Fig. 3*G*). Ablation of this region by truncation eliminated Rab7 binding altogether (Fig. S6). Expression of the full-length Rab-binding defective construct (TPC2[RBDaaa]-GFP) in *Xenopus* oocytes failed to yield as pronounced a pigmentation defect as TPC2 (Fig. 3*H*). Collectively, these data suggest that TPC-evoked pigmentation (and trafficking) defects depend upon TPC and Rab interactivity and functionality within TPC2-expressing organelles.

Contextual Expression of TPCs Underpins the Pigmentation Effect. Expression of TPC1 did not produce the trafficking or pigmentation phenotype (Fig. 3 *A* and *H*) even though both TPCs bind Rabs (Fig. 2*B*) and are expressed at similar levels (Fig. S7). Because TPC1 and TPC2 target differentially (TPC2 is predominantly lysosomal whereas TPC1 is biased toward endosomes in mammalian cells), we reasoned that the cellular locale of TPC expression was critical for evoking these outcomes. Analysis of TPC2 versus TPC1 distribution in *Xenopus* oocytes revealed that TPC2 displayed a unique polarized distribution targeting around the apex of the animal pole (Fig. 4*A*). No TPC2 immunoreactivity could be detected by immunoblotting in the vegetal half of the oocyte, generating a sharp animal–vegetal gradient of TPC2 expression (Fig. 4*B*). The polarized distribution of TPC2 was also seen with the pore mutant TPC2[L265P], but not with TPC1, which was expressed broadly throughout the cell (Fig. 4*C*). Even at the apex of the oocyte, where TPC1 and TPC2 expression overlap, the vesicular targeting profile was distinct (Fig. S8).

Next, we used mutant constructs to change the cellular expression locale of both TPC isoforms. First, TPC2 was rerouted to the cell surface by deletion of the NH_2-terminal lysosomal

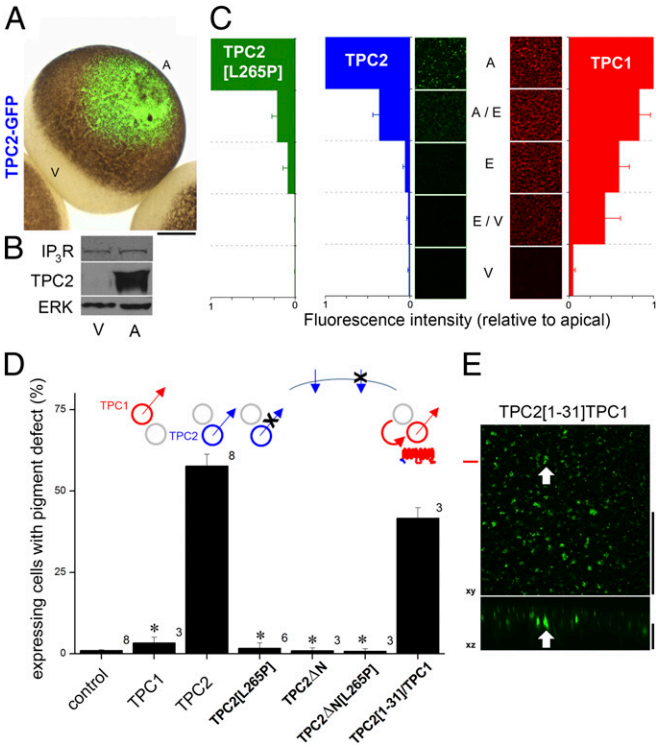

Fig. 4. Pigmentation defects depend upon contextual expression of TPC2. (*A*) Overlay of epifluorescence and brightfield images showing expression of TPC2-GFP at the apex of a *Xenopus* oocyte. (Scale bar: 250 μm.) (*B*) Western blot from vegetal (V) and animal (A) halves of a single oocyte showing expression of IP_3R1, TPC2, and ERK (loading control) confirming that TPC2 is restricted to the animal pole. (*C*) Quantification of polarity of TPC expression. Punctate expression of TPC2 and TPC2[L265P] (pore mutant) was concentrated at the top of the animal pole whereas TPC1 was expressed more broadly. Lateral (*xy*) confocal sections were captured at the same laser power within the indicated regions of the same oocyte (E, equatorial), by rotating the oocyte 45° between each image capture. Fluorescence intensity was expressed relative to the intensity recorded at the apex of the animal pole in each cell. Error bars show SEM. (*D*) Dataset scoring the proportion of TPC-expressing cells displaying pigment defects in indicated cohorts. (*Upper*) Schematics illustrate the effect of mutations on TPC distribution (TPC1, red; TPC2, blue; expressed in discrete organelles) and functionality (X represents [L265P] pore mutation). The chimeric TPC2[1-31]/TPC1 construct contains the TPC2 targeting sequence. Data from $n \geq 3$ donor frogs (numbered), with ≥50 oocytes injected per construct. Error bars show SEM, $^*P < 0.01$. (*E*) Vesicular aggregates (arrowed) in an oocyte expressing a chimeric TPC2[1-31]/TPC1 construct in lateral (xy, *Upper*) (scale bar: 35 μm) and axial (xz, *Lower*) (scale bar: 15 μm) section (at red line).

targeting sequence (TPC2ΔN). No pigment defect was observed in cells expressing TPC2ΔN (Fig. 4*D*), which acts as a functional plasma membrane channel (5). Second, we generated a chimeric construct combining a short NH_2-terminal region of TPC2 with the remaining TPC1 backbone (TPC2[1-31]/TPC1). This construct swaps the proposed NH_2-terminal lysosomal targeting region of TPC2 (5) into the TPC1 backbone. Expression of TPC2 [1-31]/TPC1 was sufficient to cause both pigment (Fig. 4*D*) and trafficking defects (Fig. 4*E*), outcomes absent in TPC1-expressing oocytes. Rerouting TPC1 into TPC2-positive organelles is therefore sufficient to yield pigmentation and trafficking outcomes seen with wild-type TPC2, but not wild-type TPC1. Therefore, contextual regulation of TPC isoforms within discrete organelles underpins the isoform specificity of these phenomena.

Regulation of NAADP-Evoked Ca^{2+} Signals by Rab GTPases. Finally, the effects of Rab inhibition on NAADP-evoked Ca^{2+} signaling was studied. NAADP-evoked responses were inhibited in HEK293 cells expressing the Rab-binding deficient mutant (TPC2[RBDaaa]-GFP) compared with wild-type TPC2-GFP (Fig. 5). NAADP-evoked Ca^{2+} release was also inhibited in TPC2-expressing cells preincubated with the Rab7 inhibitor compared with TPC2-expressing controls (Fig. 5). Therefore, NAADP signaling was impaired when Rab function or Rab/TPC2 interactivity was blocked using pharmacological or molecular approaches. We conclude that TPC2 interactivity with Rab GTPases supports NAADP-evoked Ca^{2+} signals.

Discussion

Definition of the human TPC interactome provides an unbiased insight into TPC cell biology and provides a resource helpful in the context of current controversies over how TPCs are regulated (12, 13). Guided by the interactome dataset, we explored here the unique in vivo interactions between TPC isoforms and Rab GTPases, which we discovered impacted pigmentation and trafficking dynamics in the frog oocyte. Melanin pigmentation protects cells (including frog eggs) from UV damage, and it is noteworthy that TPCs (41) and interactors evidenced here (47) are linked in genetic association studies to pigmentation defects in humans, implying an evolutionarily conserved role. These phenotypes depend on TPC2 activity and correct localization of TPC2 within the cell. Ablation of TPC2 activity, Rab interactivity with TPC2, or expressing TPC2 elsewhere within the oocyte prevented these defects (Fig. 4*A*). TPC1 did not cause these outcomes, and this isoform selectivity resulted from the differential endogenous expression locale of these channels as TPC1 recapitulated these defects when rerouted using TPC2 trafficking signals (Fig. 4 *A* and *B*). Because Rab7 activity promotes lysosomal aggregation (24) and acts as a rate-limiting step for substrate accumulation and degradation in the oocyte (48), overexpression of TPC2-scaffolded Rabs likely perturbs endomembrane dynamics to displace melanosomes at the apex of the cell over the area that correlates with the polarized cap of TPC2 expression (Fig. 3*F*). This demonstration of the association of Rabs with TPCs establishes a molecular convergence of key regulators of endolysosomal trafficking—Rab GTPases, phosphoinositides, and local ion fluxes—onto the TPC complex. Phosphoinositides regulate TPC activation and recruitment of trafficking effectors (10, 49, 50). Localized ion fluxes triggered on TPC activation may support fusogenic events (10): Fusion of endosomes and lysosomes in vitro requires a Ca^{2+} flux downstream of Rab activity (51), and reciprocally Ca^{2+} fluxes regulate Rab cycling (52). Although each regulator acts as a discrete component in the endolysosomal trafficking machinery, demonstration that this triumvirate of regulators converges upon a single molecular entity (TPCs) highlights the important cellular role of these ancient channel complexes in endolysosomal trafficking.

Consequently, changes in TPC regulation and activity may augur relevance to scenarios of lysosomal proliferation in aging and neurodegenerative states (14). This association is noteworthy given other nodes within the TPC interactome provide links with Parkinson disease: CHP is highlighted in independent genetic association studies (53, 54), and the LAT1 transporter (SLC7A5/SLC3A2) mediates L-DOPA transport. Moreover, both Rab7 and TPC2 bind to the leucine-rich repeat kinase 2 (LRRK2) (55), mutant forms of which underlie familial Parkinson disease.

In summary, proteomic analysis of TPCs evidences links with interactors that coordinate endolysosomal trafficking and membrane organization. This association may underscore a fundamental and evolutionarily conserved role of the TPC complex in trafficking and may even provide the common principle linking diverse physiological activities (glucose homeostasis, fertilization, exocytosis, and neurite outgrowth) in which NAADP has been previously implicated.

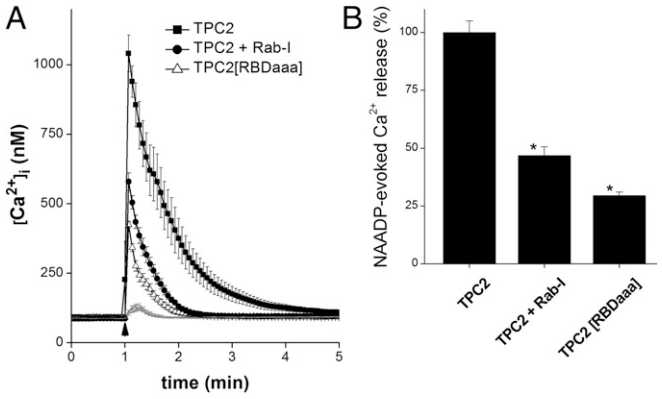

Fig. 5. Rab GTPase interactivity with TPC2 supports NAADP-evoked Ca^{2+} release. (*A*) NAADP-evoked Ca^{2+} signals in HEK293 cells transfected with TPC2-GFP (filled symbols) or the Rab-binding deficient mutant (TPC2[RBDaaa]-GFP, open symbols). Averaged Ca^{2+} responses ($n = 5$) to NAADP [injected at 1 s (arrowhead), ~10 nM final concentration] are shown together with microinjection control traces (gray). (*B*) Comparison of the peak amplitude of NAADP-evoked Ca^{2+} signals under indicated conditions. All error bars show SEM, $^*P < 0.01$.

Materials and Methods

Reagents. Several TPC constructs (MYC-, GFP-, mRFP-tagged TPC1/2) and TPC mutants (GFP-tagged TPC2ΔN, TPC2[L265P], TPC2ΔN[L265P]) were reported previously (2, 5). Primers used for cloning other constructs were as follows: MYC-tagged TPC2 NH_2-terminal (1–80 amino acids) [forward (F), ccatcgattcgaattcatggcggaaccccagg; reverse (R), gatgggatgcctcgaggttcgagtaataccgtcggtaaa] and COOH-terminal (706–754 amino acids) constructs (F, cgcctcgagcacctgcagccccttgctgggacccc; R, gcgtctagatcacctgcacagccaca), GDI2-GFP (F, taccggactcagatctatgaatgaggagtacgacgtg; R, ccgcggtaccgtcgacgtcttccccatagatgtcattc), GDP-lock [T22N] Rab7 (F, gattctggagttggtaagaactcactcatgaaccagtatg; R, catactggttcatgagtgagttcttaccaactccagaatc), and GTP-lock [Q67L] Rab7 (F, acacagcaggcctggaacggttcca; R, tggaaccgttccaggcctgctgtgt). The TPC1/2 chimera construct (TPC2[1-31]:TPC1[33-816]) was generated by sequence overlap extension using internal (F, gaagagctacctagcaaaaatgg; R, atttttgctaggtagctcttcgctgcggtaagtggtcag) and outer (F, caccatcgatatggcggaaccccag; R, aggaaggcgaacactgtcac) primer pairs to generate a cassette that was cloned into $pCS2^+$ TPC1 GFP (ClaI, BsPE1). Chemicals were from Sigma-Aldrich, with the exceptions of Ca^{2+} chelators (Invitrogen) and 2-(benzoylcarbamothioylamino)-5,5-dimethyl-4,7-dihydrothieno[2,3-c]pyran-3-carboxylic acid ("Rab-I," CID 1067700; EMD Millipore). Antibodies were as follows: GFP, MYC, β-actin, and control IgG (sc-9996, sc-8334, sc-40, sc-47778, and sc-2025/27; Santa Cruz), total ERK (05–1152; EMD Millipore), TMEM33 (SAB1102315; Sigma-Aldrich), IP_3R (*Xenopus* IP_3R1, residues 404–418), and secondary antibodies (IRDyes 680/800, LI-COR Biosciences; Alexa Fluor 680, Invitrogen).

***Xenopus* Oocyte and Mammalian Cell Culture.** Female *Xenopus* frogs (Nasco) were prepared and injected with cDNA as detailed previously (56). For confocal imaging, oocytes were imaged after 48 h (Olympus FluoView 1000 IX2). For epifluorescence imaging, oocytes were visualized using a Leica MZ16F stereomicroscope with an X-Cite 120 lightsource (EXFO Inc.), and images were captured using a QiCAM 12-bit cooled color CCD camera. Chelators and Rab inhibitor were incubated with injected oocytes for 48 h. Western blotting was performed on single oocytes using rapid transfer methods. For mammalian cell culture, human embryonic kidney (HEK293) cells and human mammary gland epithelial cells (SKBR3) were purchased

from American Type Culture Collection (ATCC) and maintained in MEM and McCoy's 5A media, respectively. All culture media (37 °C/5% CO_2) were supplemented with 10% (vol/vol) heat-inactivated FBS, 1% penicillin (100 units/mL), 1% streptomycin (100 μg/mL), and L-glutamine (290 μg/mL). For Ca^{2+} imaging, microinjection (NAADP, 1 μM in femtotips) and fura-2 experiments were performed in transfected HEK293 cells (57). Cells were inhibited with Rab inhibitor (10 μM) for 24 h before imaging.

Affinity Purification and Coimmunoprecipitation of TPC Complexes. Methods are described fully in *SI Materials and Methods*.

ACKNOWLEDGMENTS. Work was supported by National Institutes of Health Grants GM088790 (to J.S.M.) and DA035926 and DA023204 (to M.E.A.) and by Biotechnology and Biological Sciences Research Council Grant BB/G013721/1 (to S.P.). R.H. was supported by a Bogue Research Fellowship.

1. Zakon HH (2012) Adaptive evolution of voltage-gated sodium channels: The first 800 million years. *Proc Natl Acad Sci USA* 109(Suppl 1):10619–10625.
2. Brailoiu E, et al. (2009) Essential requirement for two-pore channel 1 in NAADP-mediated calcium signaling. *J Cell Biol* 186(2):201–209.
3. Calcraft PJ, et al. (2009) NAADP mobilizes calcium from acidic organelles through two-pore channels. *Nature* 459(7246):596–600.
4. Pitt SJ, et al. (2010) TPC2 is a novel NAADP-sensitive Ca^{2+} release channel, operating as a dual sensor of luminal pH and Ca^{2+}. *J Biol Chem* 285(45):35039–35046.
5. Brailoiu E, et al. (2010) An NAADP-gated two-pore channel targeted to the plasma membrane uncouples triggering from amplifying Ca^{2+} signals. *J Biol Chem* 285(49): 38511–38516.
6. Schieder M, Rötzer K, Brüggemann A, Biel M, Wahl-Schott CA (2010) Characterization of two-pore channel 2 (TPCN2)-mediated Ca^{2+} currents in isolated lysosomes. *J Biol Chem* 285(28):21219–21222.
7. Ruas M, et al. (2010) Purified TPC isoforms form NAADP receptors with distinct roles for $Ca^{(2+)}$ signaling and endolysosomal trafficking. *Curr Biol* 20(8):703–709.
8. Lee HC (2005) Nicotinic acid adenine dinucleotide phosphate (NAADP)-mediated calcium signaling. *J Biol Chem* 280(40):33693–33696.
9. Morgan AJ, Platt FM, Lloyd-Evans E, Galione A (2011) Molecular mechanisms of endolysosomal Ca^{2+} signalling in health and disease. *Biochem J* 439(3):349–374.
10. Wang X, et al. (2012) TPC proteins are phosphoinositide- activated sodium-selective ion channels in endosomes and lysosomes. *Cell* 151(2):372–383.
11. Cang C, et al. (2013) mTOR regulates lysosomal ATP-sensitive two-pore Na(+) channels to adapt to metabolic state. *Cell* 152(4):778–790.
12. Morgan AJ, Galione A (2014) Two-pore channels (TPCs): Current controversies. *BioEssays* 36(2):173–183.
13. Marchant JS, Patel S (2013) Questioning regulation of two-pore channels by NAADP. *Messenger (Los Angel)* 2(2):113–119.
14. Dickinson GD, Churchill GC, Brailoiu E, Patel S (2010) Deviant nicotinic acid adenine dinucleotide phosphate (NAADP)-mediated Ca^{2+} signaling upon lysosome proliferation. *J Biol Chem* 285(18):13321–13325.
15. Schmidt TG, Skerra A (2007) The Strep-tag system for one-step purification and high-affinity detection or capturing of proteins. *Nat Protoc* 2(6):1528–1535.
16. Lam AK, Galione A, Lai FA, Zissimopoulos S (2013) Hax-1 identified as a two-pore channel (TPC)-binding protein. *FEBS Lett* 587(23):3782–3786.
17. Demaegd D, et al. (2013) Newly characterized Golgi-localized family of proteins is involved in calcium and pH homeostasis in yeast and human cells. *Proc Natl Acad Sci USA* 110(17):6859–6864.
18. Fujii Y, et al. (2012) Surf4 modulates STIM1-dependent calcium entry. *Biochem Biophys Res Commun* 422(4):615–620.
19. Zhang S, et al. (2006) Distinct role of the N-terminal tail of the Na,K-ATPase catalytic subunit as a signal transducer. *J Biol Chem* 281(31):21954–21962.
20. Walker DS, Ly S, Lockwood KC, Baylis HA (2002) A direct interaction between $IP(_3)$ receptors and myosin II regulates $IP(_3)$ signaling in C. elegans. *Curr Biol* 12(11): 951–956.
21. Zerial M, McBride H (2001) Rab proteins as membrane organizers. *Nat Rev Mol Cell Biol* 2(2):107–117.
22. Hutagalung AH, Novick PJ (2011) Role of Rab GTPases in membrane traffic and cell physiology. *Physiol Rev* 91(1):119–149.
23. Rink J, Ghigo E, Kalaidzidis Y, Zerial M (2005) Rab conversion as a mechanism of progression from early to late endosomes. *Cell* 122(5):735–749.
24. Bucci C, Thomsen P, Nicoziani P, McCarthy J, van Deurs B (2000) Rab7: A key to lysosome biogenesis. *Mol Biol Cell* 11(2):467–480.
25. Saxena SK, Kaur S (2006) Regulation of epithelial ion channels by Rab GTPases. *Biochem Biophys Res Commun* 351(3):582–587.
26. Müller CS, et al. (2010) Quantitative proteomics of the Ca_v2 channel nano-environments in the mammalian brain. *Proc Natl Acad Sci USA* 107(34):14950–14957.
27. Zhang H, Cuevas J (2002) Sigma receptors inhibit high-voltage-activated calcium channels in rat sympathetic and parasympathetic neurons. *J Neurophysiol* 87(6): 2867–2879.
28. Su TP, Hayashi T, Maurice T, Buch S, Ruoho AE (2010) The sigma-1 receptor chaperone as an inter-organelle signaling modulator. *Trends Pharmacol Sci* 31(12):557–566.
29. Xu J, et al. (2011) Identification of the PGRMC1 protein complex as the putative sigma-2 receptor binding site. *Nat Commun* 2:380.
30. Zeng C, et al. (2007) Subcellular localization of sigma-2 receptors in breast cancer cells using two-photon and confocal microscopy. *Cancer Res* 67(14):6708–6716.
31. Ostenfeld MS, et al. (2005) Effective tumor cell death by sigma-2 receptor ligand siramesine involves lysosomal leakage and oxidative stress. *Cancer Res* 65(19): 8975–8983.
32. Vilner BJ, Bowen WD (2000) Modulation of cellular calcium by sigma-2 receptors: Release from intracellular stores in human SK-N-SH neuroblastoma cells. *J Pharmacol Exp Ther* 292(3):900–911.
33. He P, et al. (2009) High-throughput functional screening for autophagy-related genes and identification of TM9SF1 as an autophagosome-inducing gene. *Autophagy* 5(1): 52–60.
34. Tang HW, et al. (2011) Atg1-mediated myosin II activation regulates autophagosome formation during starvation-induced autophagy. *EMBO J* 30(4):636–651.
35. Ghislat G, Knecht E (2012) New Ca(2+)-dependent regulators of autophagosome maturation. *Commun Integr Biol* 5(4):308–311.
36. BasuRay S, Mukherjee S, Romero E, Wilson MC, Wandinger-Ness A (2010) Rab7 mutants associated with Charcot-Marie-Tooth disease exhibit enhanced NGF-stimulated signaling. *PLoS ONE* 5(12):e15351.
37. Brailoiu E, et al. (2005) Nicotinic acid adenine dinucleotide phosphate potentiates neurite outgrowth. *J Biol Chem* 280(7):5646–5650.
38. Gutierrez MG, Munafó DB, Berón W, Colombo MI (2004) Rab7 is required for the normal progression of the autophagic pathway in mammalian cells. *J Cell Sci* 117(Pt 13):2687–2697.
39. Pereira GJ, et al. (2011) Nicotinic acid adenine dinucleotide phosphate (NAADP) regulates autophagy in cultured astrocytes. *J Biol Chem* 286(32):27875–27881.
40. Ohbayashi N, Fukuda M (2012) Role of Rab family GTPases and their effectors in melanosomal logistics. *J Biochem* 151(4):343–351.
41. Sulem P, et al. (2008) Two newly identified genetic determinants of pigmentation in Europeans. *Nat Genet* 40(7):835–837.
42. Fukuda M, Kanno E, Ishibashi K, Itoh T (2008) Large scale screening for novel rab effectors reveals unexpected broad Rab binding specificity. *Mol Cell Proteomics* 7(6):1031–1042.
43. Subramanian VS, Marchant JS, Parker I, Said HM (2001) Intracellular trafficking/membrane targeting of human reduced folate carrier expressed in Xenopus oocytes. *Am J Physiol Gastrointest Liver Physiol* 281(6):G1477–G1486.
44. Agola JO, et al. (2012) A competitive nucleotide binding inhibitor: In vitro characterization of Rab7 GTPase inhibition. *ACS Chem Biol* 7(6):1095–1108.
45. Hooper R, Churamani D, Brailoiu E, Taylor CW, Patel S (2011) Membrane topology of NAADP-sensitive two-pore channels and their regulation by N-linked glycosylation. *J Biol Chem* 286(11):9141–9149.
46. Ward HH, et al. (2011) A conserved signal and GTPase complex are required for the ciliary transport of polycystin-1. *Mol Biol Cell* 22(18):3289–3305.
47. Hider JL, et al. (2013) Exploring signatures of positive selection in pigmentation candidate genes in populations of East Asian ancestry. *BMC Evol Biol* 13:150.
48. Mukhopadhyay A, Funato K, Stahl PD (1997) Rab7 regulates transport from early to late endocytic compartments in Xenopus oocytes. *J Biol Chem* 272(20): 13055–13059.
49. Dong XP, et al. (2010) PI(3,5)P(2) controls membrane trafficking by direct activation of mucolipin Ca(2+) release channels in the endolysosome. *Nat Commun* 1:38.
50. Jha A, Ahuja M, Patel S, Brailoiu E, Muallem S (2014) Convergent regulation of the lysosomal two-pore channel-2 by Mg^{2+}, NAADP, $PI(3,5)P_2$ and multiple protein kinases. *EMBO J* 33(5):501–511.
51. Pryor PR, Mullock BM, Bright NA, Gray SR, Luzio JP (2000) The role of intraorganellar Ca(2+) in late endosome-lysosome heterotypic fusion and in the reformation of lysosomes from hybrid organelles. *J Cell Biol* 149(5):1053–1062.
52. Parkinson K, et al. (2014) Calcium-dependent regulation of Rab activation and vesicle fusion by an intracellular P2X ion channel. *Nat Cell Biol* 16(1):87–98.
53. Lesnick TG, et al. (2007) A genomic pathway approach to a complex disease: Axon guidance and Parkinson disease. *PLoS Genet* 3(6):e98.
54. Kim JM, et al. (2011) SNPs in axon guidance pathway genes and susceptibility for Parkinson's disease in the Korean population. *J Hum Genet* 56(2):125–129.
55. Gómez-Suaga P, Hilfiker S (2012) LRRK2 as a modulator of lysosomal calcium homeostasis with downstream effects on autophagy. *Autophagy* 8(4):692–693.
56. Lin-Moshier Y, Marchant JS (2013) Nuclear microinjection to assess how heterologously expressed proteins impact Ca2+ signals in *Xenopus* oocytes. *Cold Spring Harb Protoc*, 10.1101/pdb.prot072785.
57. Brailoiu GC, Oprea TI, Zhao P, Abood ME, Brailoiu E (2011) Intracellular cannabinoid type 1 (CB1) receptors are activated by anandamide. *J Biol Chem* 286(33):29166–29174.